Journal of Zhejiang University-SCIENCE A (Applied Physics & Engineering) in press
www.jzus.zju.edu.cn; www.springer.com/journal/11582
E-mail: jzus_a@zju.edu.cn

Research Article

https://doi.org/10.1631/jzus.A2400148

Centrifuge modeling of contaminant transport in keyed sand-bentonite cutoff walls

Bo HUANG, Linfeng CAO, Jiachen GUO, Chunrui XU, Yuchao LI✉

MOE Key Laboratory of Soft Soils and Geoenvironmental Engineering, Department of Civil Engineering, Zhejiang University, Hangzhou 310058, China

Abstract: Soil-bentonite (SB) cutoff walls are commonly used as barriers in polluted areas. The embedded part of an SB wall in an aquitard is crucial for its performance. In this study, a centrifuge modeling test was carried out to investigate the effect of contact between the key and the aquitard on the migration behavior of contaminants within a sand-bentonite cutoff wall. The centrifuge was accelerated to 100g and maintained in-flight for 36 h, equivalent to 41 years of transport time in the prototype. Results showed that the contaminant concentration within the SB wall was higher downstream than in the middle in the thickness direction, and deeper regions exhibited a greater concentration than shallower ones. This concentration distribution indicated that contaminants were transported along the interface between the SB wall and the aquitard, bypassing the base of the SB wall to reach the downstream aquifer rapidly. An improved numerical simulation considering preferential interface migration was performed, which agreed with the centrifuge test results. The simulation results indicated that preferential interface migration, as a defect, significantly accelerated the speed of contaminant migration, reducing the breakthrough time of the SB wall to 1/9 of that without preferential interface migration.

Key words: Cutoff wall; Centrifuge modeling; Contaminant transport; Defect; Breakthrough time

1 Introduction

Soil-bentonite (SB) vertical cutoff walls are widely used in underground barrier isolation measures to prevent or delay contaminants from leaving the site (Ruffing et al., 2018; Cao et al., 2021). Typically, a trench measuring 0.6-1.2 m wide is excavated along the perimeter of a contaminated site and then filled with a mixture of in-situ deposits and bentonite slurry to form a flexible wall (D'Appolonia, 1980; Li et al., 2015). To reduce leakage, SB walls are usually embedded in an aquitard, like a rock or clay layer, in which the embedded part of the SB wall is called the "key." The key's performance significantly influences the service life of an SB wall (Tachavises and Benson, 1997; Lee and Benson, 2000). The design life of an SB wall in geoenvironmental control projects is typically around 30 years or even longer, as some organic contaminants have attenuation half-lives longer than 30 years (Ruffing et al., 2018). However, when a defect occurs in the key, the service life of the SB wall falls far short of its design value. Therefore, it is useful to investigate the impact of the key on contaminant transport for predicting the service life of SB walls in geoenvironmental projects.

Due to the cost and duration of field studies, few field surveys have reported observational data regarding pollutant transport in SB walls in treated contaminate sites (Ryan et al., 2022), and only few researchers have investigated the distribution of effective stress on the walls (Ryan and Spaulding, 2008; Tong et al., 2020). In laboratory studies, Lee and Benson (2000) prepared a scale model of a sandy deposit with an SB wall. They studied the influence of defects on the impermeability of the SB wall and revealed the importance of keys. However, the stress levels they tested were lower than actual, which resulted in unrealistic parameters of the SB wall or the contact state with the surrounding soil and did not

✉ Yuchao LI, liyuchao@zju.edu.cn
Bo HUANG, https://orcid.org/0000-0002-7293-8618
Linfeng CAO, https://orcid.org/0000-0001-8211-7445

Received Mar. 14, 2024; Revision accepted June 28, 2024; Crosschecked

simulate the transport of pollutants. In contrast, geotechnical centrifuge modeling tests have advantages. First, they achieve a stress level similar to that of a prototype, allowing for an accurate simulation of the parameters of the SB wall and the contact state between the SB wall and its surrounding soil. Second, centrifuge tests accelerate the transport of contaminants, making them potentially feasible for simulating long-term contaminant transport.

Previous studies have successfully modelled the migration of various pollutants in layered liners using centrifuge tests (Arulanandan et al., 1988; Knight and Mitchell, 1997; Gamerdinger et al., 2001; Hutchison et al., 2003; Soga et al., 2003; Lo et al., 2005; Timms et al., 2009; Kumar and Singh, 2012; Shu et al., 2018). However, few studies have investigated the migration of pollutants in vertical barriers using centrifuge tests. Kererat et al. (2013) conducted four experiments under 30g conditions to study the migration of light non-aqueous phase liquids (LNAPLs) in sandy sites featuring a hanging soil-cement cutoff wall. Zhan et al. (2022) performed a centrifuge experiment (100g) for 43.8 h to compare the long-term performance of loess-modified and unmodified SB walls. However, both sides of the cutoff wall were rigid porous stones instead of aquifers, which resulted in inconsistent stress between the experimental model and the field. The stress state significantly affects the contaminant transport parameters of SB walls, including their porosity and hydraulic conductivity (Filz et al., 2001; Yeo et al., 2005). In addition, the bottom of the SB walls was not embedded with an aquitard but sealed with metal slots, overlooking the influence of the key on the performance of SB walls (Tachavises and Benson, 1997; Lee and Benson, 2000). Hence, integrating the deposits surrounding an SB wall (aquifer and aquitard) into a scaled model could offer a more realistic method to emulate the working conditions of vertical barriers.

The objective of this paper is to present the results of centrifuge tests of chloride ion (Cl^-) migration in sandy sites featuring a keyed SB cutoff wall, and investigate the impact of the key on the migration of contaminants. Additionally, the similitudes of the horizontal effective stress of the SB wall are discussed. Finally, numerical analysis was conducted by applying the finite-element (FE) method, through which the migration behavior and breakthrough time in the SB wall were computed.

2 Centrifuge modeling

2.1 Scaling laws

To evaluate the similitudes of the contaminant transport process in the centrifuge modeling test, Arulanandan et al. (1988) proposed eight dimensionless numbers and discussed the conditions for their similitudes (Table 1). When the experiment uses the same soil and contaminant solution as the

Table 1 Summary of dimensionless numbers (Arulanandan et al., 1988)

Number	Formula	Commentary
Concentration	$\pi_1 = C / \rho_f$	Satisfied
Reynolds	$\pi_2 = \rho_f v_s l_p / u$	π_2<1, to keep the validity of Darcy's law
Advection	$\pi_3 = v_s t / l$	Satisfied
Diffusion	$\pi_4 = D_m t / l^2$	Satisfied
Capillary	$\pi_5 = \rho_f g l l_p / T_f$	Satisfied
Adsorption	$\pi_6 = S / \rho_f$	Equilibrium adsorption
Dynamic effects	$\pi_7 = g t^2 / l$	Laminar flow
Péclet	$\pi_8 = v_s l_p / D_m$	π_8<1, to insure similarity in model and prototype

Note: C=the concentration of contaminant in the pore water [ML^{-3}]; ρ_f=the fluid density [ML^{-3}]; v_s=the interstitial flow velocity [LT^{-1}]; l_p=the characteristic microscopic length (e.g., particle size) [L]; μ=the dynamic viscosity of the fluid [$ML^{-1}T^{-1}$]; t=the time [T]; l=the soil length e.g., particle size, the characteristic microscopic length (e.g., sample height)[L]; D_m=the aqueous molecular diffusion coefficient in porous medium [L^2T^{-1}]; g=the acceleration due to gravity [LT^{-2}]; T_f=the surface tension of the fluid particle interface [MT^{-2}]; S=the mass of the adsorbed contaminant/unit volume [ML^{-3}]

prototype and the adsorption meet equilibrium adsorption, the dimensionless numbers π_1, π_3, π_4, π_5, and π_6 are identical in the model and its prototype, but π_2 (i.e., the Reynolds number), π_7, and π_8 (i.e., the Péclet number) are not identical. Note that although the expressions π_2 and π_8 are the same as the Reynolds and Péclet numbers, respectively, they have different physical meanings in the study of similarity in pollutant transport during centrifuge testing. The π_2 represents the dynamic similarity of fluid motion (Hensley and Schofield, 1991; Zhan et al., 2022), created in a laminar scenario ($\pi_2 < 1$, to keep the validity of Darcy's law). The π_8 describes the relationship between the two dispersive phenomena of mechanical dispersion and molecular diffusion (Arulanandan et al., 1988; Cooke and Mitchell, 1991). When contaminant dispersion is dominated by the process of molecular diffusion ($\pi_8 < 1$), the dispersion can be modelled even without ensuring the similarity of π_8. The π_7 would be considered if dynamic events occurred.

In this study, the similarity of π_1, π_3, and π_4 was achieved unconditionally, while π_5, π_6, and π_7 were not relevant to this study and therefore could be ignored. The similitudes of π_2 and π_8 are discussed further in the Results and Discussion.

2.2 Experimental facilities and model configuration

In this study, the ZJU-400 centrifuge from Zhejiang University was utilized. The centrifuge model was conceptualized based on a landfill located in China. This landfill, situated in a valley, was underlain by unweathered rock that acted as a relatively impermeable layer. An SB wall was installed downstream of the landfill. The model was placed in a strongbox measuring 770 × 400 × 510 mm (length × width × height), which was divided into three sections using two 8 mm-thick perforated baffles made of acrylic. The two end sections of the strongbox were designated as water reservoirs, while the middle section housed the SB wall and the surrounding soil deposits. The schematic setup of the model is shown in Fig. 1.

The head water reservoir, accounting for 38% of the volume of the strongbox, ensured a steady upstream water level during the contaminant transport stage. The comparatively small tail water reservoir (9% of the strongbox volume) featured an overflow valve connected to its sidewall to maintain a constant downstream water level during the in-flight stage. The SB wall was located in the model's center and was 4 cm thick and 40 cm high. The aquifer and aquitard were situated on either side of the SB wall, with 34 cm and 17.5 cm thickness, respectively. The SB wall was inserted 6 cm into the aquitard at the bottom.

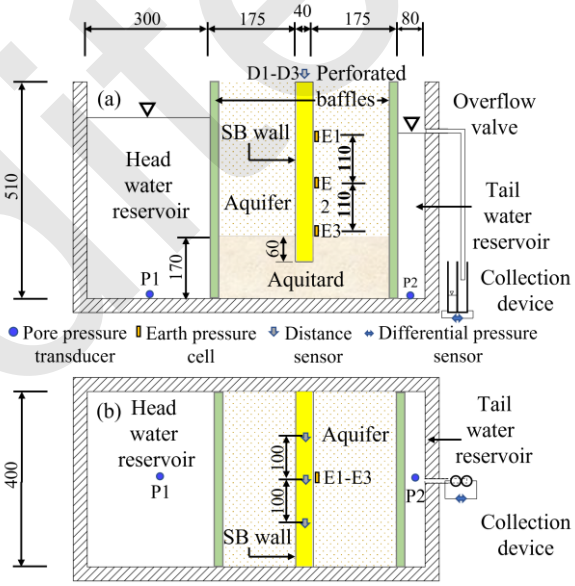

Fig. 1 Schematic diagram of the centrifuge model set-up (mm): (a) profile view; (b) plan view

2.3 Test materials and model preparation

This study used sodium chloride (NaCl) as the contaminant because Cl^- is essentially a conservative tracer (Arulanandan et al., 1988; Mckinley et al., 1998), which avoided the difficulty of achieving

Table 2 Properties of constituent soils

Soil	C_u	C_c	e_{max}	e_{min}	L_L (%)	P_I (%)	G_s
Fujian standard sand	1.7	0.96	0.85	0.52	/	/	2.64
Wyoming bentonite	/	/	/	/	342	260	2.55

Note: C_u=coefficient of uniformity; C_c=coefficient of curvature; e_{max}=maximum void ratio; e_{min}=minimum void ratio; L_L=liquid limit; P_I=plasticity index; G_s=specific gravity of soil particle

adsorption similitude in the experiment. The concentration of NaCl was set at 0.1 mol/L, which is close to the average concentration observed in field investigations conducted by Xu et al. (2019) at landfill sites. It should be noted that landfills contain other more harmful pollutants, such as organic matter and heavy metal ions, they are not conservative transport. Therefore, their breakthrough behavior may differ from Cl^-, and it is necessary to conduct further transport experiments for these pollutants.

Two different types of soils were used in this test: Fujian standard sand and Wyoming bentonite. The bentonite was a thoroughly natural Na-based bentonite commercially available from Wyo-Ben, Inc., Billings, Montana, USA. Its mineral composition, determined by X-Ray diffraction, comprised 12.3% quartz, 12.7% andesine, 3.6% illite, and 71.4% Na-montmorillonite. The bentonite's cation exchange capacity (CEC) was 79.93 meq/100 g, measured by the ammonium exchange method, and its specific surface area was 80.23 m^2/g, determined by the N_2 adsorption method. Table 2 shows their physical properties, and Fig. 2 their grain size distribution curve. The aquifer consisted exclusively of Fujian standard sand. The SB backfill and aquitard were prepared using air-dried Fujian sand, a bentonite slurry (5% bentonite in deionized water), and pure bentonite.

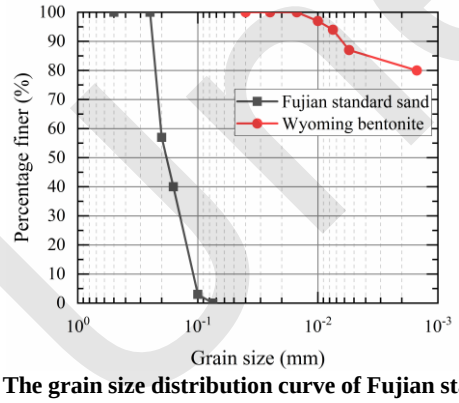

Fig. 2 The grain size distribution curve of Fujian standard sand and Wyoming bentonite

Before the model was prepared, four pairs of slots were fixed on the side of the strongbox for installing the perforated baffle and the SB wall construction mold. A 10-mesh screen (wire diameter 0.32 mm, aperture 2.3 mm) and filter paper were fixed on the side of the perforated baffle in contact with the soil to prevent the soil from entering the water tank. Two perforated baffles were then inserted, and a steel support frame was placed to maintain pressure equilibrium and prevent deformation of the water tank (Fig. 3a). Moreover, bentonite paste was applied to the walls of the soil storage area to inhibit water leakage between the soil and the strongbox.

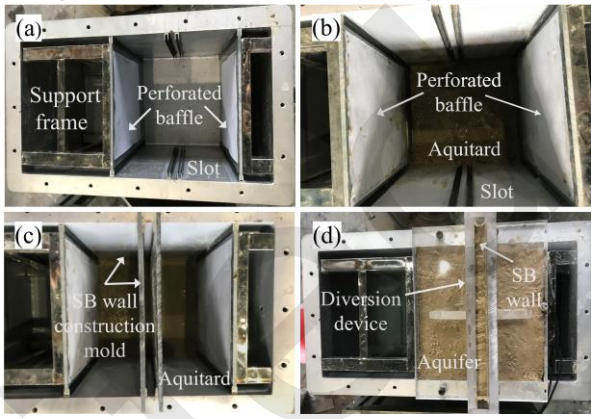

Fig. 3 Model preparation: top-view

The aquitard was prepared by a moist tamping method with five lifts, each 34 mm thick, compacted using an impact compactor plate with a surface area of 0.02 m^2 and a mass of 5 kg to achieve the desired density of 1.78 g/cm^3 (Fig. 3b).

Before installing the wall model, the SB wall construction mold with a thickness of 8 mm was inserted into the slots (Fig. 3c). Then, a 6-cm aquitard was prepared on the outer side of the SB wall construction mold to form the key. To avoid trapping air bubbles, a piping bag filled with the SB backfill was used to extrude the SB backfill from the bottom of the narrow molds while being lifted gradually. Note that this differed from field construction, in which the SB backfill is placed on a slope and displaces slurry.

The same method was used to prepare the aquifer on both sides of the SB wall with a controlled density of 1.94 g/cm^3. After completing the aquifer, the SB wall construction mold was slowly pulled out of the model. The space previously occupied by the SB wall construction mold was then filled by the sinking of the SB backfill. Finally, a diversion device was installed on the top of the strongbox to supplement SB backfill during the consolidation of the SB wall (Fig. 3d). Detailed information on the diversion device can be found in the supplementary materials. Table 3 shows the mixing proportions and physical properties of the soils after preparation.

Table 3 The mixing proportions and physical properties of the different soils

Soil	Sand (%)	Bentonite (%)	Water (%)	h_s (mm)	e_0	ρ_0 (g/cm^3)
SB backfill	68.84	3.62	27.54	125	1.22	1.73
Aquifer	90.91	0	9.09	/	0.74	1.94
Aquitard	66.66	16.67	16.67	/	1.08	1.78

Note: The proportion of each component is a mass percentage. h_s=slump; e_0=initial void ratio; ρ_0=initial density

2.4 Test materials and model preparation

In this study, four types of sensors were used: a pore pressure transducer, strain-type earth pressure cell, non-contact type laser distance sensor, and differential pressure sensor. Pore pressure transducers, with an accuracy of ±1 kPa, were placed at the bottom of the head and tail water reservoirs to monitor changes in water levels. Strain-type earth pressure cells, with an accuracy of ±2 kPa, were attached to the side of the SB wall to measure horizontal earth pressure. The method for installation of the soil pressure sensor can be found in the supplementary materials. Laser sensors, with an accuracy of ±0.05 mm, were mounted above the SB wall to monitor its settlement. Additionally, a differential pressure sensor with an accuracy of ±0.04 kPa was placed in the collection device to measure the seepage discharge. Fig. 1 provides details of the sensor installation locations during model preparation. Note that the positions of the earth pressure sensors changed due to the settlement of the soil. Therefore, their positions were remeasured after the experiment.

2.5 Test Procedure

The test was divided into three stages: consolidation, watertightness testing, and contaminant migration.

In the first stage, the model was centrifuged at 100g. The high porosity SB backfill was consolidated and supplemented with SB backfill via the diversion device. This stage lasted for over 8 h until the settlement rate of the SB wall fell below 1 mm/h, a criterion also adopted by Wang et al. (2016).

The second stage aimed to examine the watertightness between the soil and the strongbox by setting a head difference of 3 cm between the upstream and downstream. When the seepage discharge in the model was less than the calculated value of 27.36 mL/h, it indicated no significant leakage between the soil and the strongbox. Note that the calculated seepage discharge did not consider the preferential flow through the interface between the SB wall and the aquitard due to the unknown permeability of the interface, which differed from the actual situation. Additionally, due to the unknown hydraulic conductivity of the SB wall, this value was calculated using the upper limit of the SB wall's hydraulic conductivity (1×10^{-9} m/s). If the seepage discharge substantially exceeded the calculated value, the model had to be re-prepared. This stage lasted about 3 h. In this test, the actual head difference was 3.56 cm and the average seepage discharge was 24.68 mL/h. Thus, the watertightness of the model satisfied the requirements.

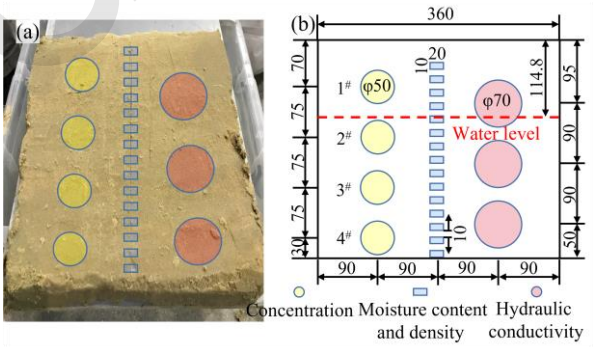

Fig. 4 Sample collection: (a) SB wall on the operating platform; (b) schematic of sampling locations (mm)

Before the start of the third stage, the deionized water in the head water reservoir was replaced with a 0.1 mol/L NaCl solution to simulate the pollution source. The expected water level difference between two reservoirs was set as 3 cm but measured 3.66 cm in practice, with a seepage discharge of 26.44 mL/h. This stage lasted 36 h. Due to an average ambient temperature of 38 ℃ in the centrifuge chamber, evaporation caused a decrease in water levels in both reservoirs. However, the unit area evaporation rates of the two reservoirs were similar, maintaining a head difference of 3.66 cm. According to P2, the down-

stream water level was 11.48 cm below the top of the SB wall at the end of the test. Photographs of the centrifuge model are shown in the supplementary materials.

3 Numerical simulation of contaminant transport for centrifuge modeling

3.1 Numerical modeling

A finite element method program, COMSOL Multiphysics 5.5, was used to investigate the transport behavior of contaminants in the centrifuge test. The convection-dispersion equation was used as the governing equation in the solute transport model, as shown in Eq. (1):

$$\frac{\partial C_{\mathrm{i}}}{\partial t}=D_{x,\mathrm{i}}\frac{\partial^2 C_{\mathrm{i}}}{\partial x^2}+D_{z,\mathrm{i}}\frac{\partial^2 C_{\mathrm{i}}}{\partial z^2}-v_{x,\mathrm{i}}\frac{\partial C_{\mathrm{i}}}{\partial x}-v_{z,\mathrm{i}}\frac{\partial C_{\mathrm{i}}}{\partial x} \quad (1)$$

where i represents ua, cw, da, and at (ua=upstream aquifer, cw=SB wall, da=downstream aquifer, at=aquitard); C_{i}=denotes the contaminant concentration of each part; $D_{x,\mathrm{i}}$ and $D_{z,\mathrm{i}}$ represent the horizontal and vertical hydrodynamic dispersion coefficients, respectively, $D_{x,\mathrm{i}}=\tau_{\mathrm{i}}D_0+\alpha_{\mathrm{i}}v_{x,\mathrm{i}}$, $D_{z,\mathrm{i}}=\tau_{\mathrm{i}}D_0+\alpha_{\mathrm{i}}v_{z,\mathrm{i}}$ (τ_{i} is the tortuosity factor, $\tau_{\mathrm{i}}=n_{\mathrm{i}}^{1/3}$ (Mott and Weber, 1991), n_{i} is the porosity of the different soils, D_0 is the aqueous molecular diffusion coefficient); α_{i} is the dispersivity; $v_{x,\mathrm{i}}$ and $v_{z,\mathrm{i}}$ are the horizontal and vertical seepage velocities, respectively.

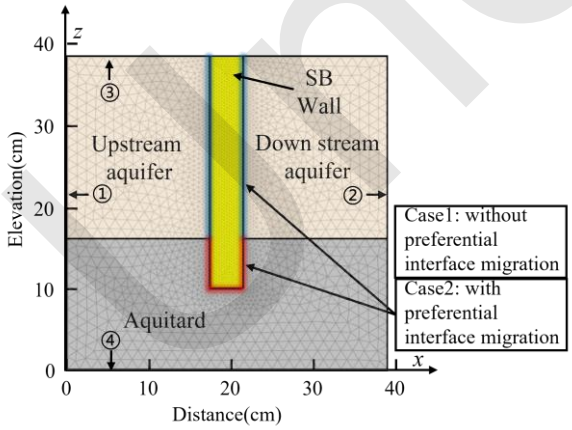

Fig. 5 2D finite-element model of centrifuge test: mesh and boundary conditions

A two-dimensional (2D) finite element model corresponding to the dimensions of centrifuge modeling was established (Fig. 5). It is important to emphasize that the numerical model used in this study was developed at the model scale rather than the prototype scale. The centrifugal acceleration *Ng* in the numerical model was set to 100g. The increase in *Ng* induced a greater pore water pressure gradient, leading to a heightened seepage velocity *v* and an increased hydrodynamic dispersion coefficient. This is the effect of *Ng* on the pollutant transport governing equation.

The concentration of sample 1#, located above the water level in the experiment, was nearly zero (Fig. 4b). This suggests that the contaminant transport in the unsaturated zone was notably slow. Therefore, for modeling simplicity, the simulation was confined to the saturated zone. Four boundaries are outlined in the equations shown in Table 4: the inflow boundary, outflow boundary, upper boundary, and lower boundary. The layer interface should comply with continuity conditions of concentration, contaminant flux, pressure, and seepage flux. The numerical model used a constant head difference h_w 3.66 cm and a constant Cl^- concentration of the head water reservoir C_0 of 0.1 mol/L. This numerical model is referred to as ***Case 1***.

Table 4 The boundary conditions of model

	Type	Contaminant transport	Seepage
①	Inflow Boundary	$C=C_0$	$P=\rho_{\mathrm{f}}Ng(H_{\mathrm{m}}-z+h_{\mathrm{w}})$
②	Outflow Boundary	$\frac{\partial C}{\partial x}=0$	$P=\rho_{\mathrm{f}}Ng(H_{\mathrm{m}}-z)$
③	Upper Boundary	$\frac{\partial C}{\partial z}=0$	$\frac{\partial P}{\partial z}=0$
④	Lower Boundary	$\frac{\partial C}{\partial z}=0$	$\frac{\partial P}{\partial z}=0$

Note: P= pore water pressure; H_{m}= model height; ρ_{f} = 993 kg/m^3 (38 ℃)

Notably, the results of ***Case 1*** on the contaminant distribution differed significantly from those of the centrifuge test (Fig. 8). The contaminant concentration within the SB wall was higher downstream than in the middle, and deeper regions exhibited a greater concentration than shallower ones. This concentration distribution indicated that pollutants did not reach the downstream aquifer via the SB wall; instead, they migrated directly from the interface between the SB wall and the aquitard, circumventing the base of the SB wall to reach the downstream aquifer. To validate

this hypothesis, a small-scale dye tracing experiment under 1g conditions using a transparent box was performed. The soil materials and preparation methods for this experiment were consistent with the centrifuge test. The results revealed that the red dye bypassed the base of the SB wall and swiftly reached the downstream aquifer (detailed information on this test can be found in the supplementary materials).

When the SB wall and aquitard in the experiment were without defects, the interface between them was likely to become the pathway with the lowest resistance to water and pollutant transport. In particular, the length of the key of the SB wall was scaled down in centrifuge tests, which means that the hydraulic path between the interfaces was also shortened relative to the field condition, resulting in a more significant preferential interface migration. Additionally, the base soil of SB mixture used in the experiment (Fujian standard sand) had a larger particle size, making the interface between the SB wall and aquitard rougher, which further promoted the generation of preferential interface migration. In subsequent studies, silt with a smaller particle size was used as the base soil of the SB mixture for centrifuge tests. The preferential interface migration then essentially disappeared when maintaining the same experimental setup, model preparation, and test procedure. Therefore, in practical engineering, when the in-situ soil has a larger particle size, such as sand, it cannot be used directly as the base soil for SB backfill. Instead, smaller particle-size silt or clay should be used as the base soil for SB backfill to prevent the generation of preferential interface migration.

To simulate preferential interface migration, Rowe and AbdelRazek (2019) introduced a transmissive layer with a high hydraulic conductivity into the numerical model. Inspired by this, we introduced transmissive layers to simulate preferential interface migration. However, the finite elements proved inadequate for calculating its effect due to the layer's extremely fine spacing compared to the model components. To address this, we adopted the approach of Mozafari et al. (2018) using "fractures" to simulate preferential interface migration. Within COMSOL, fractures are not represented as physical entities but are simplified as internal boundaries, offering an effective solution to multi-scale challenges. The governing equation of contaminant transport and water flow in a fracture can be found in the supplementary materials.

Therefore, this study adopted the internal boundaries of fractures to simulate preferential interface migration. In the numerical model of ***Case 2***, the internal boundaries of fractures were added at the interface between the SB wall and the surrounding soil. Briefly, this study involved two numerical models, ***Case 1*** without preferential interface migration and ***Case 2*** with preferential interface migration, to simulate Cl^- transport in the centrifuge test.

3.2 Parameters in the numerical model

The numerical simulation requires two sets of input parameters:

1. Transport parameters of each soil, used in the two numerical models (***Case 1*** and ***Case 2***), are shown in Table 5 and Fig. 6 (with the vertical axis representing the elevation of the numerical model). The porosity n_i and hydraulic conductivity k_i of each soil were determined through after-test sampling results. Notably, the parameters of the aquifer and aquitard were set as constant, considering their negligible change with depth. The dispersivity α_i of soils was found by reference to by Gelhar et al. (1992) and Wang et al. (2016). The aqueous molecular diffusion coefficient D_0 of Cl^- was obtained from the transport parameter manual (Yaws, 2014).

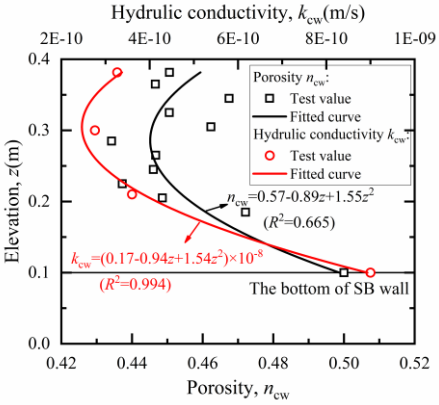

Fig. 6 The hydraulic conductivity and porosity of the SB wall in the numerical model

2. Transport parameters of each fracture were used only in ***Case 2*** (Table 6). The pore diameter d_f of each fracture was determined by fitting the seepage discharge (26.44 mL/h) measured during the contaminant transport phase. The porosity n_f of different fractures was taken as 1, referring to Zhan et al.

(2023). The aqueous molecular diffusion coefficient $D_{0,f}$ of different fractures was the same as in Table 5. The dispersivity α_f of different fractures was obtained by fitting the concentration distribution of contaminants.

Table 5 Transport parameters in the numerical model

Soil	n_i	k_i (m/s)	D_0 (m^2/s)	α_i (m)
Aquifer	0.36	2.1×10^{-5}	2.78×10^{-9} [a]	0.5 [b]
SB wall	$n_{cw}(z)$	$k_{cw}(z)$	2.78×10^{-9} [a]	0.0068 [c]
Aquitard	0.49	1×10^{-12}	2.78×10^{-9} [a]	0.0068 [c]

Note: data were measured and calculated in this study except as follows: a. Yaws (2014); b. Gelhar et al. (1992); c. Wang et al. (2016)

Table 6. Transport parameters of each fracture

The type of fracture	d_f (mm)	n_f	$D_{0,f}$ (m^2/s)	α_f (m)
SB wall-aquifer	0.048	1	2.78×10^{-9}	3
SB wall-aquitard	0.0076	1	2.78×10^{-9}	1

Note: d_f = pore diameter of the fracture; n_f = porosity of the fracture; $D_{0,f}$ =aqueous molecular diffusion coefficient of contaminants in the fracture; α_f = dispersivity of the fracture

4 Results and discussion

4.1 Horizontal effective stress

Fig. 7 shows the normalized horizontal effective stress σ'_h/H of the SB wall from this and other published studies, and the detailed information on these SB walls is presented in Table 7. Notably, the dimensions of the SB wall in this study were converted to a prototype scale. The horizontal effective stress of the SB wall in this study showed an initial increase and a subsequent decrease with depth, which was consistent with some field measurements (Ryan and Spaulding, 2008; Tong et al., 2020). This horizontal stress distribution can be attributed to arching and lateral squeezing effects during the consolidation of the SB wall (Ruffing et al., 2010; Li et al., 2015; Ke et al., 2018). In contrast, Zhan et al. (2022) conducted a centrifuge model test using rigid porous stones to support an SB wall. This method prevented the inward movement of the trench side walls, resulting in little variation in wall stress with depth. Furthermore, the σ'_h/H in this study exceeded that measured by Tong et al. (2020) but was consistent with the findings of Ryan and Spaulding (2008). This disparity may be attributable to the differences in the base soil of the SB wall.

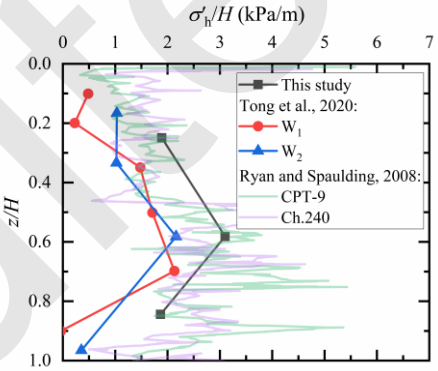

Fig. 7 Comparison of results from different studies of horizontal effective stress in an SB wall after normalization

The stress state of SB backfills significantly impacts the transport parameters of SB walls, such as porosity and hydraulic conductivity (Filz et al., 2001; Yeo et al., 2005). Therefore, it is crucial to ensure the similarity between the stress states of SB walls in both centrifuge models and prototypes for the accurate simulation of pollutant transport.

Table 7 Comparison of SB walls in this and other published studies

SB wall	H (m)	b (m)	B_C	Base soil	Measuring method	Reference
This study	38.5	4	5.0	Sand	Earth pressure cells	/
W_1	6	0.6	4.7	Silty clay	Earth pressure cells	Tong et al. (2020)
W_2	10	0.6				
CPT-9	35	0.8	/	Sand	CPTU	Ryan and Spaulding (2008)
Ch.240	30	0.8				

Note: H=depth of the SB wall; b= width of the SB wall; B_C= bentonite content. The method for converting CPTU results to effective horizontal stress is given by Ke et al. (2018).

4.2 Similitudes of contaminant transport

The similitudes of π_2 and π_8 are discussed in this section.

$$\pi_2 = \frac{\rho_f v_s l_p}{\mu} \tag{2}$$

where ρ_f=993 kg/m^3, v_s=Q/ (An_{cw}), in which Q is the seepage discharge, Q =26.44 mL/h, A is the flow area of the SB wall, A=756.72 cm^2, and n_{cw} is the porosity of the SB wall. Considering the variation of porosity with depth, the average value was taken, n_{cw}=0.45; l_p is the mean particle diameter (Arulanandan et al., 1988), l_p =0.14 mm; μ=0.68×10^{-3} Pa s.

$$\pi_8 = \frac{v_s l_p}{D_m} \tag{3}$$

where D_m=$\tau_{cw}D_0$, in which τ_{cw} is the tortuosity factor of the SB wall, τ_{cw}=$n_{cw}^{1/3}$ (Mott and Weber, 1991; Li et al., 2022), and D_0 is the aqueous molecular diffusion coefficient, D_0=2.78×10^{-9} m^2/s.

The π_2 and π_8 were calculated as 4.42×10^{-5} and 0.011, respectively. As they were less than 1, they met the similarity requirement.

4.3 Migration behavior of chloride ions through the SB barrier system

Fig. 8 illustrates the distribution of Cl$^-$ concentration across the width of the SB wall, obtained from after-test sampling results after 36 h transport (scattered points) and simulated outcomes from ***Case 1*** and ***Case 2*** (dashed and solid lines, respectively). The horizontal X-axis represents the SB wall thickness L_{cw}, where L_{cw}=0 denotes the location of contact between the SB wall and the upstream aquifer. The longitudinal Y-axis shows the relative Cl$^-$ concentration C_{cw}/C_0.

The Cl$^-$ concentration across the SB wall increased progressively with depth according to the test results. Near the inlet of the SB wall, the C_{cw}/C_0 at depths 2$^{\#}$, 3$^{\#}$, and 4$^{\#}$ were 0.21, 0.46, and 0.48, respectively, while at the outlet, the values were 0.067, 0.19, and 0.23. Given the threshold for a breakthrough at the outlet, C_{cw}/C_0=0.1, as Zeng et al. (2022) noted, the deeper part of the SB wall (3$^{\#}$ and 4$^{\#}$) had breached the threshold after 36 h. Hence, the lower part of the SB wall was considered the weakest part of the vertical barrier, requiring measures to improve performance. However, the Cl$^-$ concentration along with the thickness direction of the SB wall at each depth decreased initially and then increased. This distribution diverged from the results of analytical solutions based on the convection-diffusion governing equation, which anticipates a decline in pollutant concentration as the distance from the pollution source increases (Acar and Haider, 1990; Rubin and Rabideau, 2000; Li et al., 2017).

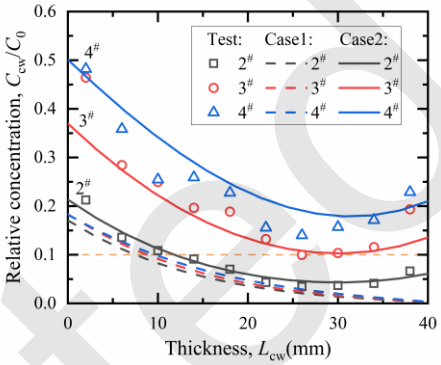

Fig. 8 Cl$^-$ concentration distribution of simulation and test

The simulation results showed a significant difference between ***Case 1***, which did not consider preferential interface migration, and the experimental findings. Specifically, ***Case 1*** exhibited much smaller Cl$^-$ concentrations and did not increase in the thickness direction. In contrast, ***Case 2***, which considered preferential interface migration, closely resembled the centrifuge test results. In the experiment, Cl$^-$ rapidly migrated along the interface between the SB wall and the aquitard, passing through the bottom of the SB wall and reaching the downstream aquifer, resulting in a higher concentration at the outlet of the SB wall than in the middle. This accounts for the concentration distribution of pollutants inside the SB wall in Fig. 8. The discovery warrants scrutiny, as preferential pathways in the field-constructed wall would represent a significant defect, potentially seriously reducing the performance of the SB wall.

Fig. 9 shows the simulation results of the Cl$^-$ contaminant plume in ***Case 2*** at different times, with the green line denoting the C_i/C_0=0.1 contour. Within the vertical barrier system, preferential pathways at the interface between the SB wall and the aquitard resulted in a seepage velocity at the base of the aquifer that exceeded that in its shallower regions. This phenomenon led to rapid migration of Cl$^-$ downstream from the bottom of the aquifer (Fig. 9 a). After 5.20 h, the Cl$^-$ concentration front reached the SB wall and rapidly transported along the aquitard-SB wall

interface (Fig. 9 b). By 13.80 h, the Cl^- concentration front reached the downstream aquifer at point B (Fig. 9 c). At 26.20 h, the Cl^- concentration front reached the tailwater reservoir, and "U"-shaped contaminant plumes emerged in the SB wall (Fig. 9 d).

Based on numerical simulation, the Cl^- breakthrough point of the SB barrier system occurred at the junction (point *B*) where the SB wall, aquitard, and downstream aquifer intersect. The breakthrough time of the SB barrier system was 13.80 h, which equated to 15.75 years in the prototype. Notably, the breakthrough time was only 1/9 of that without preferential interface migration (118.20 h).

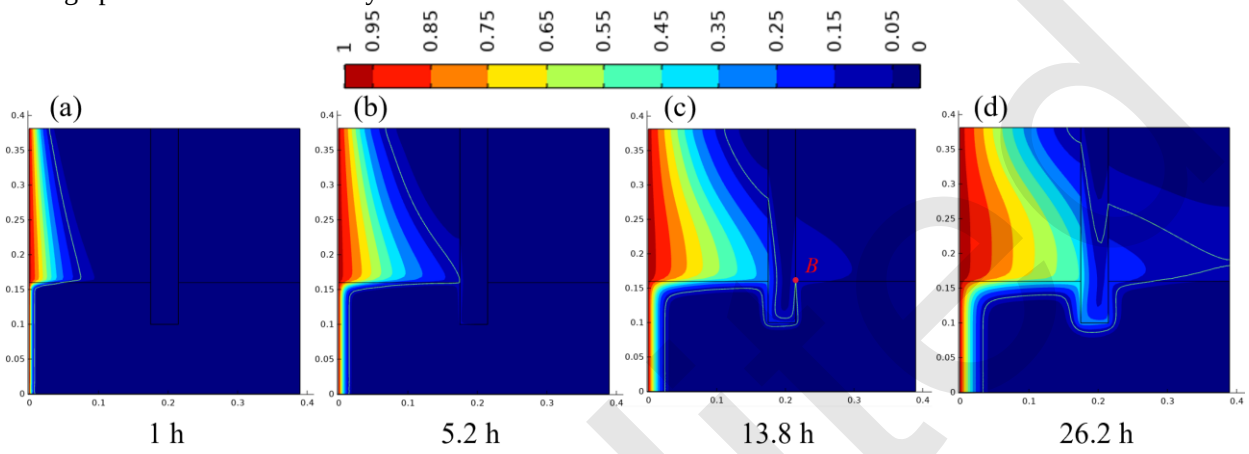

Fig. 9 Numerical simulation results for the Cl^- contaminant plume in the model at different times (C_i/C_0)

5 Conclusions

Based on the centrifuge modeling test and numerical simulations, the following conclusions were drawn:

(1) The horizontal effective stress of the SB wall in the centrifuge modeling showed an initial increase and then a decrease with depth, which is consistent with some field measurements. The similarity in stress states ensured that the transport parameters (such as porosity and hydraulic conductivity) of the SB wall and the contact state between the SB wall and its surrounding soil were consistent with the prototype.

(2) In the vertical SB barrier system, preferential interface migration occurred and significantly affected the migration behavior of contaminants. The contaminants migrated rapidly along the interface of the SB wall and aquitard, bypassing the bottom of the SB wall and reaching downstream. This observation differed from a traditional migration pathway. The preferential interface migration, as a defect, greatly accelerated the migration speed of contaminants, reducing the breakthrough time of the SB wall to 1/9 of that without preferential interface migration, which deserves attention in practical applications.

(3) An internal boundary called a "fracture" was used in the numerical model to simulate the interface preference migration. The simulation results agreed with those from the centrifuge test, affirming the viability of this simulation approach.

(4) The base soil of the SB wall used in the experiment (Fujian standard sand) had a larger particle size, making the interface between the SB wall and aquitard rougher, which promoted the generation of preferential interface migration. Therefore, in practical engineering, when the in-situ soil is sand with a larger particle size, it cannot be directly used as the base soil for an SB wall. Instead, smaller particle-size silt or clay should be used to serve as the base soil for SB backfill to prevent the generation of preferential interface migration.

Acknowledgments

The authors gratefully acknowledge funding for this work from the Ministry of Science and Technology of China (2018YFC1802304), National Natural Science Foundation of China (51988101 and 42077241) and Natural Science Foundation of Zhejiang Province (LCZ19E080002).

Author contributions

Yu-Chao Li designed the research. Lin-Feng Cao processed the corresponding data. Lin-Feng Cao wrote the first draft of the manuscript. Jia-Chen Guo and Chun-Rui Xu

helped to organize the manuscript. Bo Huang revised and edited the final version.

Conflict of interest

The authors declare that they have no known competing financial interests or personal relationships that could have appeared to influence the work reported in this paper.

References

Acar YB, Haider L, 1990. Transport of low-concentration contaminants in saturated earthen barriers. *Journal of Geotechnical Engineering-Asce*, 116(7):1031-1052. https://doi.org/10.1061/(ASCE)0733-9410(1990)116:7(1031)

Arulanandan K, Thompson PY, Kutter BL, et al., 1988. Centrifuge modeling of transport processes for pollutants in soils. *Journal of Geotechnical Engineering-Asce*, 114(2):185-205. https://doi.org/10.1061/(ASCE)0733-9410(1988)114:2(185)

ASTM (American Society for Testing and Materials), 2019. Standard test methods for laboratory determination of water (moisture) content of soil and rock by mass, ASTM D2216. ASTM, USA. https://doi.org/10.1520/D2216-19

ASTM (American Society for Testing and Materials), 2016. Standard test methods for measurement of hydraulic conductivity of saturated porous materials using a flexible wall permeameter, ASTM D5084. ASTM, USA. https://doi.org/10.1520/D5084-16A

ASTM (American Society for Testing and Materials), 2021. Standard test methods for laboratory determination of density and unit weight of soil specimen, ASTM D7263–21. ASTM, USA. https://doi.org/10.1520/D7263-21

Cao BY, Xu J, Wang F, et al., 2021. Vertical barriers for land contamination containment: A review. *International Journal of Environmental Research and Public Health*, 18(23) https://doi.org/10.3390/ijerph182312643

Cooke B, Mitchell RJ, 1991. Physical modelling of a dissolved contaminant in an unsaturated sand. *Canadian Geotechnical Journal*, 28(6):829-833. https://doi.org/10.1139/t91-100

Dappolonia DJ, 1980. Soil-bentonite slurry trench cutoffs. *Journal of the Geotechnical Engineering Division-Asce*, 106(4):399-417. https://doi.org/10.1061/AJGEB6.0000945

Filz GM, Henry LB, Heslin GM, et al., 2001. Determining hydraulic conductivity of soil-bentonite using the api filter press. *Geotechnical Testing Journal*, 24(1):61-71. https://doi.org/10.1520/GTJ11282J

Gamerdinger AP, Kaplan DI, Wellman DM, et al., 2001. Two-region flow and decreased sorption of uranium (vi) during transport in hanford groundwater and unsaturated sands. *Water Resources Research*, 37(12):3155-3162. https://doi.org/10.1029/2001WR000247

Gelhar LW, Welty C, Rehfeldt KR, 1992. A critical-review of data on field-scale dispersion in aquifers. *Water Resources Research*, 28(7):1955-1974. https://doi.org/10.1029/92WR00607

Hensley PJ, Schofield AN, 1991. Accelerated physical modeling of hazardous-waste transport. *Geotechnique*, 41(3):447-465. https://doi.org/10.1680/geot.1991.41.3.447

Hutchison JM, Seaman JC, Aburime SA, et al., 2003. Chromate transport and retention in variably saturated soil columns. *Vadose Zone Journal*, 2(4):702-714. https://doi.org/10.2136/vzj2003.7020

Ke H, Tong X, Li YC, et al., 2018. Force equilibrium–based model for predicting stresses in soil-bentonite cutoff walls. *Journal of Geotechnical and Geoenvironmental Engineering*, 144(2):04017112. http://dx.doi.org/10.1061/%28ASCE%29GT.1943-5606.0001821

Kererat C, Sasanakul I, Soralump S, 2013. Centrifuge modeling of lnapl infiltration in granular soil with containment. *Journal of Geotechnical and Geoenvironmental Engineering*, 139(6):892-902. https://doi.org/10.1061/(ASCE)GT.1943-5606.0000754

Knight MA, Mitchell RJ, 1997. Modelling of light nonaqueous phase liquid (lnapl) releases into unsaturated sand. *Canadian Geotechnical Journal*, 33(6):913-925. https://doi.org/10.1139/t96-121

Kumar RP, Singh DN, 2012. Geotechnical centrifuge modeling of chloride diffusion through soils. *International Journal of Geomechanics*, 12(3):327-332. https://doi.org/10.1061/(ASCE)GM.1943-5622.0000139

Lee T, Benson CH, 2000. Flow past bench-scale vertical ground-water cutoff walls. *Journal of Geotechnical and Geoenvironmental Engineering*, 126(6):511-520. http://dx.doi.org/10.1061/(ASCE)1090-0241(2000)126:6(511)

Li YC, Cleall PJ, Wen YD, et al., 2015. Stresses in soil-bentonite slurry trench cut-off walls. *Geotechnique*, 65(10):843-850. https://doi.org/10.1680/jgeot.14.P.219

Li YC, Chen GN, Chen YM, et al., 2017. Design charts for contaminant transport through slurry trench cutoff walls. *Journal of Environmental Engineering*, 143(9). https://doi.org/10.1061/%28ASCE%29EE.1943-7870.0001253

Li JS, Jiang WH, Ge SQ, et al., 2022. Coupled model for consolidation and organic contaminant transport in gmb/ccl composite liner under non-isothermal distribution condition. *Computers and Geotechnics*, 150, 104893. https://doi.org/10.1016/j.compgeo.2022.104893

Lo IMC, Zhang JH, Hu LM, 2005. Centrifuge modeling of cadmium migration in saturated and unsaturated soils. *Soil & Sediment Contamination*, 14(5):417-431. https://doi.org/10.1080/15320380500180440

Mckinley JD, Price BA, Lynch RJ, et al., 1998. Centrifuge modelling of the transport of a pulse of two contaminants through a clay layer. *Geotechnique*, 48(3):421-425. https://doi.org/10.1680/geot.1998.48.3.421

Mott HV, Weber WJ, 1991. Diffusion of organic contaminants through soil bentonite cutoff barriers. *Research Journal of the Water Pollution Control Federation*, 63(2):166-176. https://www.jstor.org/stable/25043972

Mozafari B, Fahs M, Ataie-Ashtiani B, et al., 2018. On the use of comsol multiphysics for seawater intrusion in fractured coastal aquifers. E3S Web of Conferences, 54:00020.

https://doi.org/10.1051/e3sconf/20185400020
Rowe RK, Abdelrazek AY, 2019. Effect of interface transmissivity and hydraulic conductivity on contaminant migration through composite liners with wrinkles or failed seams. *Canadian Geotechnical Journal*, 56(11):1650-1667. https://doi.org/10.1139/cgj-2018-0660
Rubin H, Rabideau AJ, 2000. Approximate evaluation of contaminant transport through vertical barriers. *Journal of Contaminant Hydrology*, 40(4):311-333. https://doi.org/10.1016/S0169-7722(99)00060-1
Ruffing DG, Evans JC, Malusis MA, 2010. Prediction of earth pressures in soil-bentonite cutoff walls. GeoFlorida 2010: Advances in Analysis, Modeling & Design, p.2416-2425. https://doi.org/10.1061/41095(365)245
Ruffing D, Evans J, Coughenour NJI, 2018. Soil-bentonite slurry trench cutoff wall longevity. International Foundation Congress and Equipment Expo, p.214-223. https://doi.org/10.1061/9780784481608.021
Ryan CR, Spaulding CA, 2008. Strength and permeability of a deep soil bentonite slurry wall. Geocongress 2008: Geotechnics of waste management and remediation, p.644-651. https://doi.org/10.1061/40970(309)81
Ryan CR, Ruffing D, Evans J, 2022. Soil Bentonite Slurry Trench Cutoff Walls: History, Design, and Construction Practices. In Geo-Congress 2022, p. 89-99. https://doi.org/10.1061/9780784484050.010
Shu S, Zhu W, Wang SW, et al., 2018. Leachate breakthrough mechanism and key pollutant indicator of municipal solid waste landfill barrier systems: Centrifuge and numerical modeling approach. *Science of the Total Environment*, 612:1123-1131. http://dx.doi.org/10.1016/j.scitotenv.2017.08.185
Soga K, Kawabata J, Kechavarzi C, et al., 2003. Centrifuge modeling of nonaqueous phase liquid movement and entrapment in unsaturated layered soils. *Journal of Geotechnical and Geoenvironmental Engineering*, 129(2):173-182. https://doi.org/10.1061/(ASCE)1090-0241(2003)129:2(173)
Tachavises C, Benson CH, 1997. Hydraulic importance of defects in vertical groundwater cut-off walls. In situ remediation of the geoenvironment conference, p. 168-180.
Timms W, Hendry MJ, Muise J, et al., 2009. Coupling centrifuge modeling and laser ablation inductively coupled plasma mass spectrometry to determine contaminant retardation in clays. *Environmental Science & Technology*, 43(4):1153-1159. https://doi.org/10.1021/es8020414
Tong X, Li YC, Ke H, et al., 2020. In situ stress states and lateral deformations of soil bentonite cutoff walls during consolidation process. *Canadian Geotechnical Journal*, 57(1):139-148. https://doi.org/10.1139/cgj-2018-0503
Wang YZ, Chen YM, Xie HJ, et al., 2016. Lead adsorption and transport in loess-amended soil-bentonite cut-off wall. *Engineering Geology*, 215:69-80. https://doi.org/10.1016/j.enggeo.2016.11.002
Xu HQ, Shu S, Wang SW, et al., 2019. Studies on the chemical compatibility of soil-bentonite cut-off walls for landfills. *Journal of Environmental Management*, 237:155-162. https://doi.org/10.1016/j.jenvman.2019.02.051
Yaws CL, 2014. Transport properties of chemicals and hydrocarbons. translators, William Andrew, p.704-705.
Yeo SS, Shackelford CD, Evans JC, 2005. Consolidation and hydraulic conductivity of nine model soil-bentonite backfills. *Journal of Geotechnical and Geoenvironmental Engineering*, 131(10):1189-1198. https://doi.org/10.1061/(ASCE)1090-0241(2005)131:10(1189)
Zeng X, Su J, Wang HY, et al., 2022. Centrifuge modeling of chloride ions completely breakthrough kaolin clay liner. *Sustainability*, 14(12), 6976. https://doi.org/10.3390/su14126976
Zhan LT, You YQ, Zhao R, et al., 2022. Centrifuge modelling of lead retardation in soil-bentonite cut-off walls. *International Journal of Physical Modelling in Geotechnics*, 23(4):166-179. https://doi.org/10.1680/jphmg.21.00007
Zhan LT, Cao LF, Zhao R, et al., 2023. Performances of the soil-bentonite cutoff wall composited with geosynthetic clay liners: Large-scale model tests and numerical simulations. *Sustainability*, 15(3), 1886. https://doi.org/10.3390/su15031886

Electronic supplementary materials

Sections 2.3, 2.4, 2.5 and 3.1

中文概要

题　目： 嵌入式砂-膨润土防污阻隔墙污染物运移的离心模拟

作　者： 黄博、曹林峰、郭嘉琛、徐春瑞、李育超

机　构： 浙江大学，建筑工程学院，软弱土与环境土工教育部重点实验室，中国杭州 310058

目　的： 嵌入式土-膨润土防污阻隔墙的嵌入部分对其服役性能至关重要。本文通过开展离心模型试验，探讨嵌入部分对污染物迁移的影响，以期为嵌入式土-膨润土防污阻隔墙的施工设计提供指导。

创新点： 1. 首次通过离心模型试验模拟了嵌入式土-膨润土防污阻隔墙内的污染物运移；2. 通过在数值模拟中添加裂隙这一内部边界条件，成功模拟了污染物的界面优势运移，使得模拟结果与试验结果吻合。

方　法： 1. 通过离心模型试验，获得嵌入式土-膨润土防污阻隔墙服役 36 小时（相当于原型 41 年）后的污染物浓度分布；2. 通过分析模型的渗漏量和阻隔墙内污染物浓度分布，探究阻隔墙嵌入部分与弱透水层界面处污染物的运移行为；3. 通过小尺度染料示踪试验，验证界面优势运移的存在；4. 通

过考虑界面优势运移的数值模拟，验证所提方法的可行性，并探究嵌入式土-膨润土防污阻隔墙的击穿行为和服役寿命。

结　论： 1. 阻隔墙的水平有效应力随深度先增加后减小，这与一些现场测量结果一致；2. 在阻隔墙嵌入部分与弱透水层之间的界面存在污染物的优势运移，污染物沿着界面迅速运移，绕过阻隔墙的底部并到达下游；3. 在数值模型中使用裂缝这一内部边界来模拟界面优势运移，模拟结果与离心试验结果较为吻合；4.界面优势运移作为一种缺陷，大大加快了污染物的运移速度，将阻隔墙的击穿时间缩短到没有界面优势运移时的 1/9；5.在实际工程中，当原位土壤为粒径较大的砂土时，应使用粒径较小的粉土或粘土作为土-膨润土防污阻隔墙的基土，以防止界面优势运移的产生。

关键词： 防污阻隔墙；离心模拟；污染物迁移；缺陷；击穿时间